Hannes Vennekate

II. Physikalisches Institut

— Universität Göttingen —

Bachelor Thesis:

Second Sound as Cavity Diagnostic Tool

Zweiter Schall zur Diagnose von Kavitäten

by Hannes Vennekate

II.Physik-UniGö-Bach-2009/04

Working Time:	April, 14^{th} – July, 20^{th} 2009
Advisor:	Dr. Michael Uhrmacher
First Referee:	Prof. Dr. Arnulf Quadt
Second Referee:	Prof. Dr. Ariane Frey
External Referee:	Prof. Dr. Eckhard Elsen

Contents

I. Theory **9**

1. Motivation **11**

2. Particle Acceleration in Cavities **13**
2.1. Principles 13
2.2. The Pill Box Model and different Modes 15
2.3. Why Superconductivity 17

3. Real Cavities – The TESLA Project and ILC **21**
3.1. TESLA – ILC – XFEL 21
3.2. The TESLA Cavities 22
3.3. Accelerating Field Gradient and Limits of Superconductivity 23

4. Cavity Diagnostics **27**
4.1. Reasons for Superconductivity Breakdowns 27
4.2. Thermal Mapping 29
4.3. Second Sound 30
4.3.1. The Effect of Second Sound 30
4.3.2. The Idea of Second Sound as a Cavity Diagnostic Tool 30
4.4. Oscillating Superleak Transducers – OSTs 32

II. Simulation **33**

5. Simulation with MATLAB **35**
5.1. Systematic Approach 35
5.1.1. Creating a TESLA Cavity 35
5.1.2. Concept of Simulating Second Sound 36
5.1.3. Creating Quench Spots 37
5.1.4. Detectors – OSTs 38
5.1.5. Computing the Traces 39
5.1.6. Contribution of Errors 41
5.2. Analysis 42
5.2.1. Signals per Event 42
5.2.2. Events with two Signals 43

5.2.3. Events with three or more Signals 47
5.2.4. Statistical Analysis 48

6. Conclusion and Outlook **53**
6.1. Conclusions 53
6.2. Outlook 54

Bibliography **57**

Abstract

This thesis deals with a new kind of quality diagnostic tool for superconducting radio frequency cavities of high energy particle accelerators. It is supposed to trace down imperfections which lead to local quenches. The first part describes the method developed and first tested at Cornell University, Ithaca, New York, which is based upon the quantum mechanical effect of "Second Sound". In the second part, numerical simulations are presented, which were performed with a TESLA cavity. They demonstrate that for a given realistic geometry 2×6 *detectors are sufficient, to reconstruct the location of a quench spot with a precision of about* $4 - 5\,mm$.

Part I.

Theory

Chapter 1.

Motivation

The history of particle physics is closely linked to the progress in the development of particle accelerators. From the first ray tubes, in which J.J. Thomson discovered the very first known elementary particle – the electron – in 1897, to contemporary accelerators at CERN (Conseil Européen pour la Recherche Nucléaire), Fermilab and all around the globe. The levels of energy and momentum provided by these apparatures, have been responsible for the very ability to discover new particles and physics.

This thesis deals with a new method for the important quality control of future superconducting accelerator cavities, since the diagnosis of industrial produced cavities is of growing importance in the race for higher accelerating field gradients.

The initiation of this method took place at Cornell University, Ithaca, New York [22]. It combines the effect of "Second Sound" as a form of heat transport in liquid superfluid helium – which is going to be explained later on – and the fact that nearly all superconducting cavities in contemporary accelerators are cooled with liquid helium. This thesis will focus on the TESLA type, where nine of these cavities are combined in one element, as done by the Cornell collaboration in late 2008 [22]. These TESLA cavities will be part of the future X-Ray Free-Electron Laser – XFEL – at DESY, Hamburg and will hopefully play an important role in constructing the International Linear Collider – ILC. Therefore, any improvement in their quality inspection makes sense as they represent the superconducting accelerator technology at the current state of the art.

Chapter 2.

Particle Acceleration in Cavities

2.1. Principles

All kinds of cavities have been created and improved to be used for particle acceleration. At first one might ask why to use wave guides for accelerating particles. The answer, however, is already given by the device's name: Wave guides are necessary for a zero-loss wave propagation of an electromagnetic wave, used to accelerate and focus a particle beam. Taking the electric wave equation inside a wave guide for a better explanation of its advantages into account one gets:

$$\Delta\vec{E} = \frac{1}{c^2}\frac{\partial^2}{\partial t^2}\vec{E}$$

If we separate the spatial and the temporal part we obtain:

$$\hookrightarrow \qquad \vec{E}(\vec{r},t) = \vec{E}_r(\vec{r})\mathrm{e}^{\mathrm{i}\omega t}$$

$$\Rightarrow \qquad \Delta\vec{E} - \frac{\omega^2}{\mathrm{c}^2}\vec{E} = \Delta\vec{E} + k^2\vec{E} = 0$$

Convetionally, the z-axis is considered to be the beam axis. Its separated wave equation is given by:

$$\Delta E_z = -k^2 E_z$$

If assumed to be separable into the following:

$$E_z(\vec{r}) = f_x(x)f_y(y)f_z(z)$$

we get:

$$f_x'' f_y f_z + f_x f_y'' f_z + f_x f_y f_z'' = -k^2 f_x f_y f_z$$

$$\Rightarrow \qquad \frac{f_x''}{f_x} + \frac{f_y''}{f_y} + \frac{f_z''}{f_z} = -k^2$$

With the EULARIAN ansatz

$$f_i = f_{0i} \mathrm{e}^{\mathrm{i}k_j j} \qquad j \in \{x, y, z\}$$

the equation becomes:

$$k_x^2 + k_y^2 + k_z^2 = k^2$$

If we define

$$k_c := k_x^2 + k_y^2$$

we are able to give an expression for k_z:

$$\begin{aligned} & & k_z &= \sqrt{k^2 - k_c^2} \\ \Rightarrow & & f_z &= f_{z0} \mathrm{e}^{\mathrm{i}z\sqrt{k^2-k_c^2}} \\ \Rightarrow & & f_z'' &= -k_z^2 f_z \end{aligned}$$

By multiplication with $f_x f_y$, we get;

$$\Rightarrow f_z'' f_x f_y = \frac{\partial^2}{\partial z^2} E_z = -k_z^2 e_z = -k_z f_x f_y f_z$$

which gives us a wave equation for E_z:

$$\Rightarrow \qquad \frac{\partial^2}{\partial z^2} E_z + k_z^2 E_z = 0$$

With its solution:

$$\Rightarrow \qquad E_z = E_{z0} \mathrm{e}^{\mathrm{i}k_z z}$$

From this follows, that:

$$k_c^2 > k^2 \quad \Rightarrow \quad k_z \in \mathrm{i}\,\mathbb{R}$$

leads to a damping of the electric field, while the case

$$k_c^2 < k^2 \quad \Rightarrow \quad k_z \in \mathbb{R}$$

describes the postulated zero-loss propagation.

With the relation $\frac{k}{2\pi} = \frac{1}{\lambda}$ we are able to form an expression for the wavelength of the z-component λ_z:

$$\Rightarrow \quad \frac{1}{\lambda^2} = \frac{1}{\lambda_z^2} + \frac{1}{\lambda_c^2} \tag{2.1}$$

$$\Rightarrow \quad \lambda_z^2 \left(\frac{1}{\lambda^2} - \frac{1}{\lambda_c^2} \right) = 1$$

$$\Rightarrow \quad \lambda_z^2 = \frac{\lambda^2}{1 - \left(\frac{\lambda}{\lambda_c}\right)^2}$$

$$\Rightarrow \quad \lambda_z = \frac{\lambda}{\sqrt{1 - \left(\frac{\lambda}{\lambda_c}\right)^2}} \quad > \lambda$$

Hence the z-wavelength of an undamped propagation is always bigger than λ itself. Another inequality can be deduced with the relation of the frequency and λ:

$$\omega = \frac{2\pi \mathrm{c}}{\lambda}$$

$$\overset{2.1}{\Rightarrow} \quad \frac{\omega^2}{(2\pi \mathrm{c})^2} = \frac{1}{\lambda_z^2} + \frac{1}{\lambda_c^2} = \frac{k_z^2}{(2\pi)^2} + \frac{1}{\lambda_c^2}$$

$$\Rightarrow \quad \omega = \mathrm{c} \cdot \sqrt{k_z^2 + \left(\frac{2\pi}{\lambda_c}\right)^2}$$

$$\hookrightarrow \quad v_\varphi = \frac{\omega \lambda_z}{2\pi} = \mathrm{c}\, \lambda_z \cdot \sqrt{\frac{1}{\lambda_z^2} + \frac{1}{\lambda_c^2}}$$

$$= \mathrm{c} \cdot \sqrt{1 + \left(\frac{\lambda_z}{\lambda_c}\right)^2} \quad > \mathrm{c}$$

So the phase velocity v_φ is greater than the velocity of light! (See [21])

2.2. The Pill Box Model and different Modes

For the acceleration of a particle beam, the phase velocity in z-direction has to be less than c, therefore linear accelerator structures (the most common nowadays) normally have periodic irises (or other wave obstacles) to form standing waves of certain lengths. These standing waves exist with different modes of their frequency. The most common mode of radio frequency (rf) for acceleration however is the π-mode, where the distance between two irises or the length of one cavity equals half a wavelength ($d = \frac{\lambda}{2}$). Further modes like the $\frac{1}{3}\pi$-mode result in different peak fields in the individual cells, whereas the π-mode produces the same field gradient in every cell. Figure 2.1 shows a schematic of

the decrease of phase velocity compared to the speed of light, achieved by the installation of diaphragms.

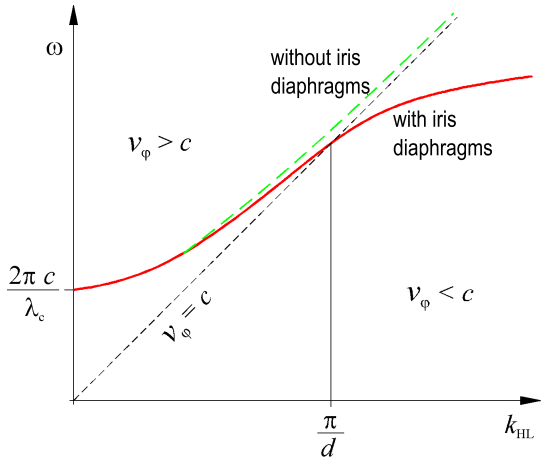

Figure 2.1.: Phase velocity with and without iris diaphragms, see [21]

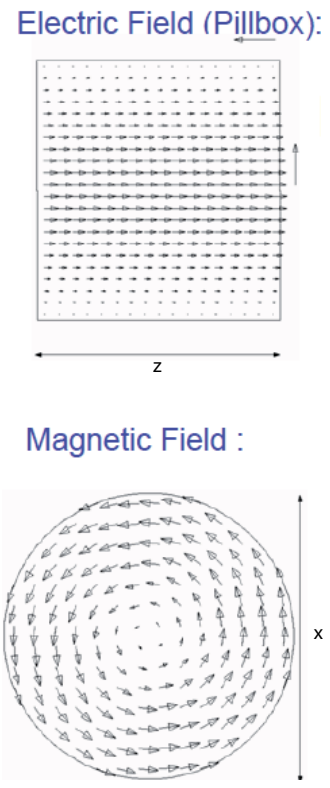

Figure 2.2.: TM_{010} mode in a pill box model, a) side view b) top view, see [11]

To explain the field distributions in a cavity, one uses the simple "pill box" model, a very primitive concept used ([8]) to explain the functionality of a cavity (an intuitive comparison might be a coke @3.95GHz). To adjust, for instance, a standing wave in a structure, it is important to choose one of the electric and magnetic field modes as well. There are in general two basic kinds of modes, the transverse electric modes – TE – (often used by klystrons to drive the cavities) and the transverse magnetic modes – TM, which are mainly responsible for particle acceleration. Due to the fundamental relationships between the electric and magnetic field, a transverse mode of one component results in the other one being the only field with a longitudinal component as shown in figure 2.2.
The fundamental TM_{010} mode in a "pill box" is given by

$$E_z = E_0 J_0 \left(\frac{2.405\, r}{R} \right) \mathrm{e}^{\mathrm{i}\omega t}$$

for the longitudinal component of the electric field, while $H_z = 0$ (and J_0 is the zeroth order BESSEL function). This is the reason why only TM modes are used for acceleration, since a (charged) particle requires an accelerating electric field in the z-direction to increase its velocity/momentum. The indices of the modes give the number of sign changes of E_z in φ-, r- and z-direction, further modes are given for example in [8].

2.3. Why Superconductivity

While superconducting magnets have become standard when high energies are required the choice between normal and superconducting cavities for modern particle accelerators is in some cases not yet clear. Even for the future ILC, concepts of normal conducting cavities have been proposed, as the current CLIC (Compact Linear Collider) draft, which favors copper cavities (at a gradient of $150\frac{\mathrm{MV}}{\mathrm{m}}$ and a concept of collider *and* drive beam). Presently, however, superconducting cavities of the former TESLA (TeV Energy Superconducting Linear Accelerator) project have been proposed for the ILC. A brief consideration of the advantages of superconductivity in this application seems to be useful. To compare normal and superconducting cavities, the point of interest is their electrical resistivity, since the resistivity is linked to the energy-loss during operation.

First of all one has to consider the resistance of a normal conductor in an rf environment as every cavity is operated with such frequencies. If we use MAXWELL'S equations we will find that for an alternating electric field with $\varepsilon\,\omega \ll \sigma$ ($\omega \mathrel{\hat{=}}$ frequency $= 2\pi\, f$, $\varepsilon \mathrel{\hat{=}}$ dielectric constant, $\sigma \mathrel{\hat{=}}$ conductivity):

$$\begin{aligned}\Delta\vec{E} &= \mathrm{i}\mu_0\mu_r\sigma\omega\vec{E}\\ &= \tau^2\vec{E}\\ \tau &:= \sqrt{\mathrm{i}\mu_0\mu_r\sigma\omega}\end{aligned}$$

And analogously for the current density $\vec{j} = \sigma\vec{E}$:

$$\Delta\vec{j} = \tau^2\vec{j}$$

If we take, for instance, a conductor placed in the positive octant ($\mathbb{R}^3$) and an electric field alternating in the y-z-plane we find:

$$\begin{aligned} & E_z = E_{z0}\exp\left(-x\sqrt{\mathrm{i}\mu_0\mu_r\sigma\omega}\right)\\ \wedge\quad & j_z = j_{z0}\exp(-\tau x)\\ \hookrightarrow\quad & \sqrt{i} = \frac{1}{2}\sqrt{2} + \frac{1}{2}\,\mathrm{i}\sqrt{2}\end{aligned}$$

$$\Leftrightarrow \qquad E_z = E_{z0}\left(\underbrace{\exp(\mathrm{i}x\sqrt{\pi\mu_0\mu_r\sigma f})}_{\text{Oscillation}} \cdot \underbrace{\exp(x\sqrt{\pi\mu_0\mu_r\sigma f})}_{\text{Decay}}\right)$$

$$\wedge \text{ analogously for} \qquad j_z = j_{z0}\left(\exp(\mathrm{i}x\sqrt{\pi\mu_0\mu_r\sigma f}) \cdot \exp(x\sqrt{\pi\mu_0\mu_r\sigma f})\right)$$

Due to the exponential decay the field only penetrates the conductor to a certain "skin depth":

$$\delta := (\pi\mu_o\mu_r\sigma f)^{-\frac{1}{2}}$$

(For example for the superconductor niobium δ is typically in the range of several nm, see [13].)

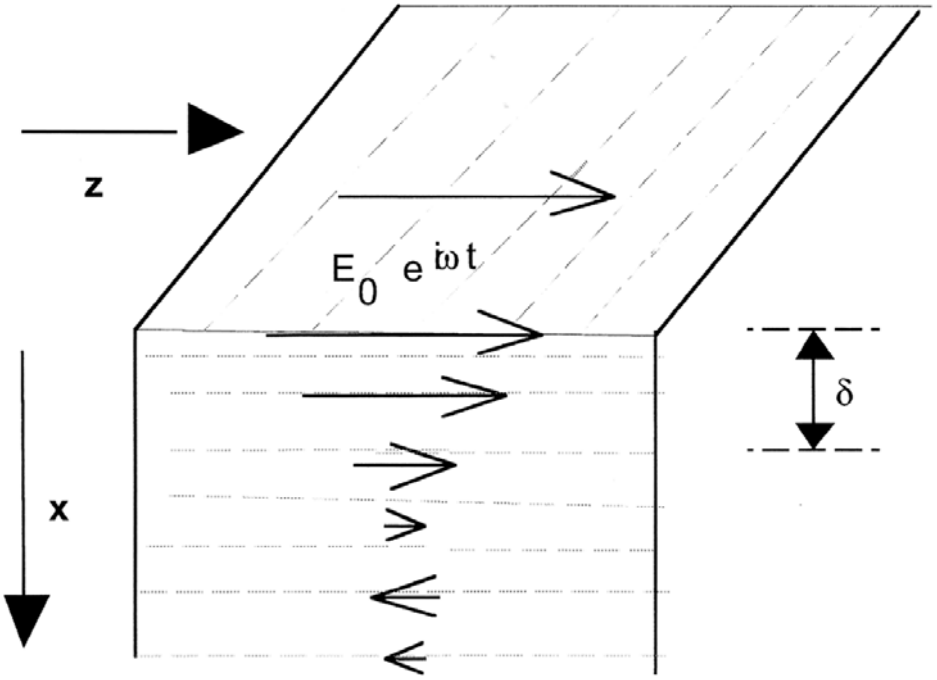

Figure 2.3.: "Penetration of rf field into normal conductor to a skin depth δ" [8]. The surface of the conductor is in the y-z-plane while the skin depth refers to the x-axis

Via the relation for j_z the surface resistance can be obtained as:

$$I = \int_0^\infty j_z \,\mathrm{d}x = \int_0^\infty j_{z0}\exp(-\tau x)\,\mathrm{d}x$$
$$= \frac{j_{z0}}{\tau}$$

$$\Rightarrow \qquad R_s = \mathfrak{Re}\left\{\frac{E_0}{I}\right\} = \mathfrak{Re}\left\{\frac{\tau}{\sigma}\right\}$$
$$= \sqrt{\pi\mu_0\mu_r\sigma f}\cdot\sigma^{-1} = \frac{1}{\sigma\delta}$$
$$\Rightarrow \qquad R_s \sim f^{\frac{1}{2}}$$

So the (surface) resistance of a normal conductor shows a proportional behavior to the square root of the frequency, which is important in an rf structure. According to the BCS theory and various experiments, the resistance of a superconductor in a dc field vanishes, but this is different in an ac field. Because of the inertia of COOPER pairs – the charge carriers in a superconductor – a non-zero resistance is created. The COOPER pairs cannot shield the external field perfectly, hence an internal field is created, which is proportional to the change of the magnetic field:

$$\vec{E}_{int} \sim \frac{dH}{dt} \sim H\omega$$

The current density is again proportional to this field times the number of the remaining normal conducting electrons:

$$j_{int} \sim E_{int}\cdot n_{e^-}$$

The energy loss or dissipated power relates to $E_{int}\cdot j_{int}$, therefore

$$\hookrightarrow \qquad P_{int} \sim E_{int}\cdot j_{int} \sim \omega^2 H^2 n_{e^-}$$
$$\wedge \qquad P_{int} = \frac{1}{2}R_s H^2$$
$$\Rightarrow \qquad R_s \sim \omega^2 n_{e^-}$$

Below its critical temperature T_c the number of unpaired electrons is given by

$$n_{e^-} \sim \exp\left(-\frac{\Delta}{k_b T}\right)$$

Where Δ defines the energy gap at the superconductor's FERMI level [19]. Hence the rf resistance of a superconductor has two important characteristics:

$$R_s \sim \omega^2 \qquad \text{and} \qquad R_s \sim \mathrm{e}^{-\frac{1}{T}}$$

Niobium for example, an important superconducting material for cavities (used in the TESLA cavities), has a surface resistance of: (See [8, 14])

$$R_s = 2\cdot 10^{-4}\frac{1}{T}\left(\frac{f}{1.5}\right)^2 \exp\left(-\frac{17.67}{T}\right)$$

Comparing the orders of magnitude of normal and superconductors, due to the temperature dependency of the superconductor's (sc) resistance a clear difference becomes visible. While for a typical normal conductor the resistance is of the order of several mΩ, the sc structures are of the order of some nΩ. This behavior leads to the major advantage of superconducting cavities. For efficiency discussions it might be argued that it is quite expensive to cool down a structure with liquid helium, as necessary for all superconductors presently in use. But the values of surface resistance and the fact that a higher resistance means a quick transformation of electrical energy into heat, make its advantage more obvious. The effort to cool a normal conducting cavity at high energy levels – so simply keeping it from melting – becomes very costly. The decrease of energy loss, i.e. warming, outweighs the cost of low temperature cooling. The sc cavities need to be cooled down once, assuming the machine keeps running, then the effort to keep them cool is less than for normal conducting cavities, because of their higher resistance.

The electrical power loss due to resistivity heating is no longer available for the beam. Hence more power is needed to get the same beam energy. So the difference in efficiency between normal and superconducting cavities can be summarized in one sentence: "In a superconducting linear collider the conversion of primary electrical power into beam power is about twice as efficient than in a normal-conducting machine." [15]

Chapter 3.

Real Cavities – The TESLA Project and ILC

3.1. TESLA – ILC – XFEL

TESLA – TeV Energy Superconducting Linear Accelerator – has been a project for a future linear electron/positron collider with an included free electron laser. The concept was proposed 2000 and until then had undergone about a decade of preplanning and meetings, starting with a workshop in 1990 [2]. The project has been divided into two separate parts, the linear accelerator and the free electron laser. In 2003, the German Federal Ministry of Education and Research decided to build only the free electron laser as a European cooperation – the X-Ray Free Electron Laser XFEL – at DESY, Hamburg, Germany, while the idea of a future linear collider turned into the ILC project within the particle physics community. The important fact is that probably both of these projects will be provided with TESLA cavities. A short summary of the accelerator physics related attributes of both projects shows the different requirements concerning the technology of the two projects. The different gradients of these cavities depend on the cavity's quality, while a higher quality also requires solid quality control methods.

	XFEL	ILC
Number of TESLA cavities	928	16000
Gradient in $\frac{\mathrm{MV}}{\mathrm{m}}$	23.6	31.5
Active Length in km	≈ 1	≈ 22
Energy in GeV	20	500

Table 3.1.: Comparision of XFEL and ILC, see [5, 12]

3.2. The TESLA Cavities

The TESLA cavities themselves for pragmatic reasons consist of a nine-cell array. Within a long linear collider, the optimum is to keep the row of accelerating cells as long as possible without interruption. But the longer a row of cells in a single cavity gets, the higher the risk of trapping higher order modes (HOM) in the cells. Additionally, the field becomes more sensitive to cavity frequency errors.

Higher order modes are a serious topic to deal with during the development phase of the cavity's geometry. These modes of "higher" order than the intended π-mode get excited in the cells and, as mentioned above, may get trapped inside the structure if not extracted in time. Therefore the line of cells needs to be periodically interrupted by so called HOM-couplers. These kinds of antennas, often in perpendicular position in front and at the end of one resonator, try to "suck" the HOMs out of the structure by resonating to their frequencies and so offering them an easy way out. This is one reason why the number of cells per resonator is limited. Furthermore, input couplers are needed, which depend on energy, frequency etc. on every x cell and it is also obvious, that one cannot operate an infinite setup of cells with just one power source (klystron).

Altogether to operate an alignment of cavities a lot of different things are needed at periodic intervalls. Couplers to establish the connection between the cavities. Klystrons are used to create the standing electromagnetic waves inside the cells, where input couplers connect these to the cells themselves and so on. In the case of the TESLA cavities concepts to reduce the number of repetitive elements have already been proposed and taken into consideration. For example so called "superstructures" are described in [17].

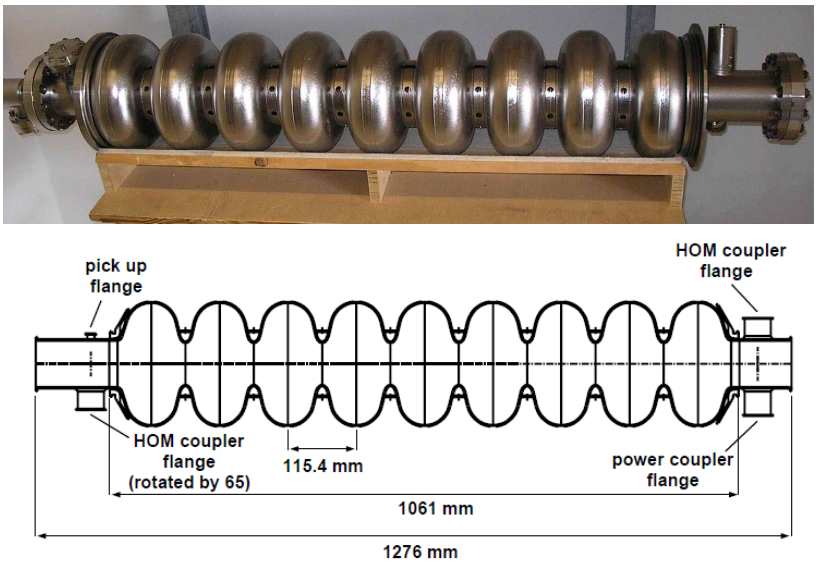

Figure 3.1.: A TESLA cavity in a picture and scheme. Notice the stiffening rings added between the cells for enhanced mechanical stability. [2, 10]

The raw material of the TESLA cavities is pure niobium which is a type-II superconductor. Because of its relatively high critical temperature of 9.2 K – the highest of all pure elements [19] – and its other favorable characteristics as a superconducting material, niobium is the state of the art in superconducting accelerator physics (in alloys also for superconducting magnets).

In operation two general factors describing the efficiency and quality of a niobium cavity are of major interest, the Residual Resistance Ratio (RRR) an the quality factor Q_0. (Further characteristics are also of importance, like the shunt impedance, but will not be discussed within the framework of this thesis.)

RRR: The residual resistance ratio is defined as [8]

$$RRR := \frac{\text{Resistivity @300 K}}{\text{Residual resistivity at low temperatures before superconducting state}}$$

and is a measurement of the purity of a metal. Typical values for niobium are $250 - 300$ [13].

Q_0: The quality factor for cavities is the ratio of the energy stored, E_s, and the power dissipated, P_d, per cycle times the frequency, ω, of the rf field

$$Q_0 := \frac{E_s}{P_d} \cdot \omega$$

thus it indicates how long the energy remains within a cavity. The quality factor in general describes the magnitude of the damping of an oscillator. Since quality factors are rather high for niobium cavities[1], the latter are ideal elements for efficient particle acceleration. Although one has to mention that these values are only attained by a high standard manufacturing process and rigorous quality standards/controls.[2]

3.3. Accelerating Field Gradient and Limits of Superconductivity

When talking about the performance of a cavity, the figure of merit is the accelerating field gradient in $\frac{\text{MV}}{\text{m}}$. This gradient can be calculated with the voltage seen by the charged particle when travelling through a cavity in z-direction:

$$V_c = \left| \int_0^d E \, \mathrm{d}z \right|$$

[1] In 2000, the TESLA collaboration demanded factors of $\geq 5 \cdot 10^9$ and today even levels of 10^{10} or 10^{11} [13] seem reasonable.

[2] Accelerator physicists like to compare these quality standards to "normal" oscillators like a church bell, which would chime for hundreds of years after one excitation at such a Q_0 factor.

The field is thus given by the alternating field component along the z-axis:

$$\begin{aligned} \Rightarrow \qquad V_c &= \left| \int_0^d E_{z0} \cdot \mathrm{e}^{\mathrm{i}\frac{\omega}{\mathrm{c}}z} \,\mathrm{d}z \right| \\ &= E_{z0} \cdot \left| \int_0^d \mathrm{e}^{\mathrm{i}\frac{\omega_0}{\mathrm{c}}z} \,\mathrm{d}z \right| \\ &= dE_{z0} \cdot \frac{\sin\left(\frac{\omega_0 d}{2\mathrm{c}}\right)}{\frac{\omega_0 d}{2\mathrm{c}}} \\ &= dE_{z0}T \end{aligned}$$

In the pill box model in TM_{010}-mode the factor T becomes $\frac{2}{\pi}$, so that the accelerating field E_{acc} is given by:

$$E_{acc} = \frac{V_c}{d} = E_{z0}T = \frac{2E_{z0}}{\pi} \left[\frac{\mathrm{V}}{\mathrm{m}}\right]$$

This quantity characterizes the cavity's ability to accelerate particles. Various levels of those gradients are in use as the space available for machines differs and the need for higher energies increases. For example the current niobium coated copper cells of the LHC have a gradient of $5\,\frac{\mathrm{MV}}{\mathrm{m}}$ while the future CLIC is supposed to run at a gradient of $150\,\frac{\mathrm{MV}}{\mathrm{m}}$ as mentioned in chapter 2. The TESLA cavities were designed to run in their test facility at a gradient of at least $15\,\frac{\mathrm{MV}}{\mathrm{m}}$ and which is supposed to be raised to $23.6\,\frac{\mathrm{MV}}{\mathrm{m}}$ at the XFEL and to $31.5\,\frac{\mathrm{MV}}{\mathrm{m}}$ at the ILC (see 3.1).

This brings us to the limits of superconducting rf structures. First of all no superconductor will run in its superconducting state above its critical temperature, therefore good an reliable cryomodules are needed. But in addition, magnetic fields cause the superconductivity to collapse as well. [19]

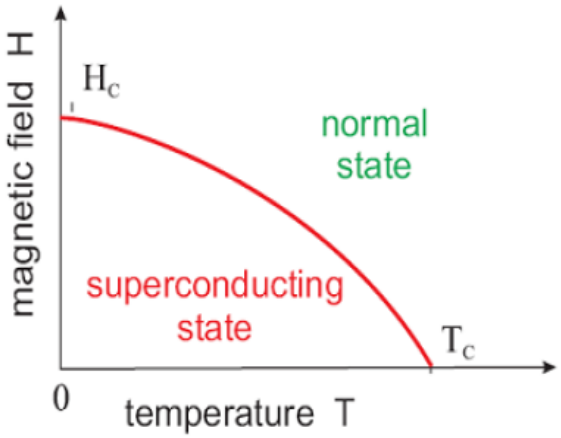

Figure 3.2.: Scheme of the limits of superconductivity [20]

According to the BCS-theory, there is a difference in the free energy of the superconducting and the normal conducting state; Cooper pairs are more highly ordered than normal conducting electrons. But if the Cooper pairs have to flow into the penetration zones of an external magnetic field to expel it, they gain energy. At a certain field H_c (thermodynamical critical field [8]), they reach the level of the normal conducting electrons and the magnetic flux can enter the conductor.

In an rf environment additional thought needs to be spent on the scale of time. For example the amount of time for forming vortexes in the conductor is about $\approx 10^{-7}\,\mathrm{s}$ while the period of the rf field

may be a lot shorter. Therefore a very strong rf field is beneficial to this limit, as higher critical magnetic fields are reachable. But in practice, the limitations of a sc cavity are caused by "quenching" (breakdown of superconductivity). These quenches are usually connected to impurities and imperfections in the superconducting material. But one has to take into account that even theoretically the fields are limited to certain values in a superconductor (niobium: $\approx 200\,\mathrm{mT}$). As the accelerating electric field is linked to the maximum magnetic field, the maximally reachable gradient is limited by H_c as well, depending on the type of superconductor and quality of the cavity's fabrication. Niobium for example will probably not be usable for gradients $> 55 - 60\,\frac{\mathrm{MV}}{\mathrm{m}}$ according to current knowledge [13].

Chapter 4.

Cavity Diagnostics

4.1. Reasons for Superconductivity Breakdowns

There is a number of phenomena which may cause a superconducting resonator to quench and lose its superconductivity.

Figure 4.1 shows a summary sketch of the most important types of cavity breakdowns.

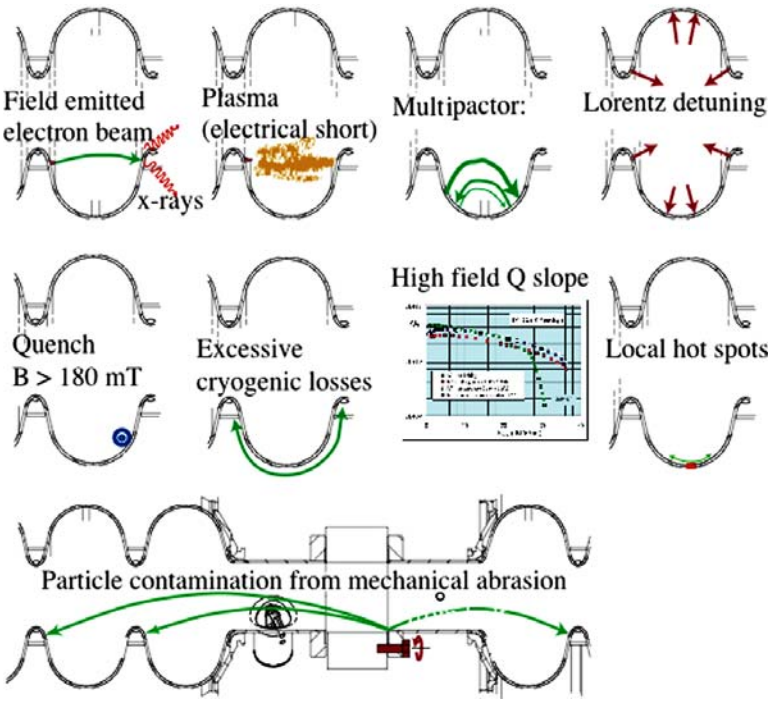

Figure 4.1.: Possible failures of a cavity, limiting its gradient [9]

As many threats for the stability of the cavity's superconducting operation exist, a lot of methods are usually applied on a cavity to keep it from failing. For example multipacting, avalanche-like electron emissions, resonating to the rf field's frequency, can be prevented by certain cell shapes [18]. And Lorentz detuning of the structure is for example fought against with additional stiffening rings between the cells (see 3.1).

Since a chain is only as strong as its weakest link, a cavity's gradient is determined by the effect which occurs at the lowest gradient. Hence a combination of all kinds of gradient improving treatments is the key to a stable operation at high levels.

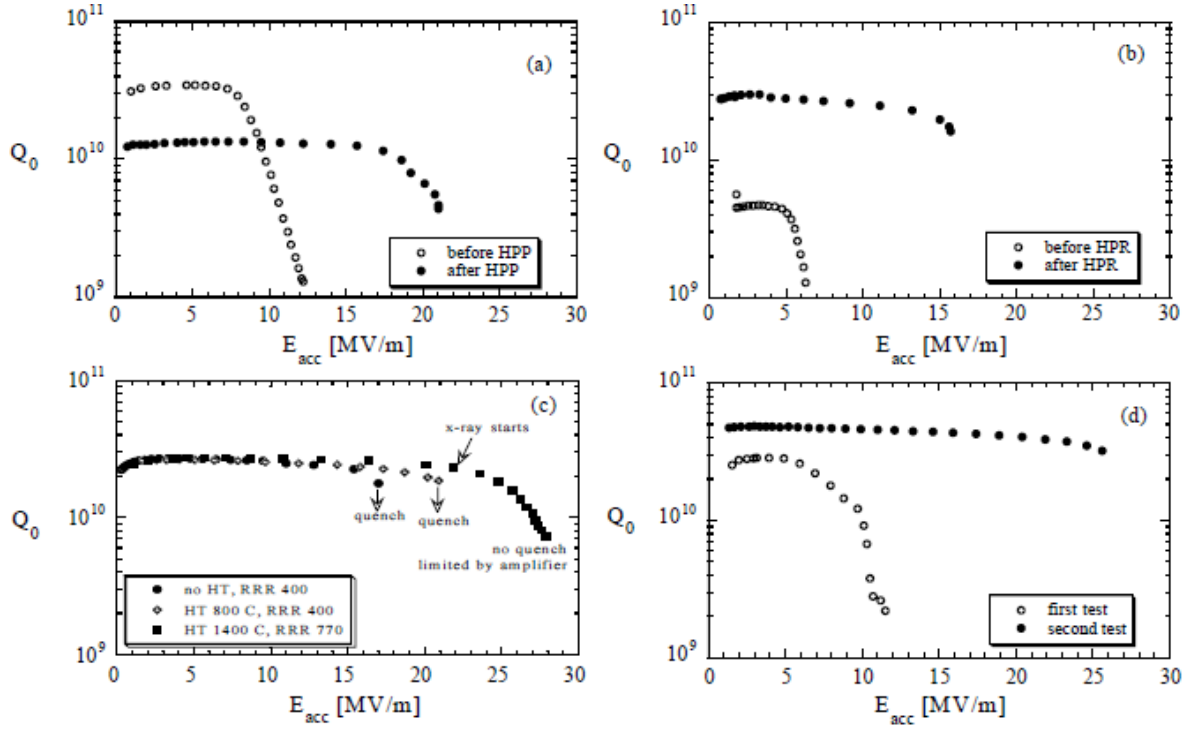

Figure 4.2.: Gradient Improvements through cavity treatment

Figure 4.2 from the TESLA collaboration [10] gives example values achieved by common treatments like:

a) high power processing (HPP)

b) high pressure water rinsing (HPR)

c) heat treatment (HT)

d) buffered chemical polishing (BCP)

One can easily see from these examples that the treatments often result in satisfactory improvements. Still in general all impurities and imperfections cause critical areas for superconductivity and are therefore the basic reason for quenches.

It is important to improve the quality diagnosis along with the cavity treatment. Besides rf measurements, which often give rather general information about one resonator's performance as a whole, temperature mapping has become one of the mainstays of cavity diagnosis.

4.2. Thermal Mapping

To gain local information about imperfections and energy losses of a cavity, the use of arrays of thermocouplers has beacome a common method. For low field and low rf frequency studies, methods with rotating chains of carbon resistors moving around the cavity's cell are useful and state of the art. For higher fields and frequencies this method is impractical, due to the fact that the according structures are cooled with superfluid helium @ $\leq 2\,\mathrm{K}$ in which the thermometers have to be put in.

Fixed thermometers are of a greater efficiency for such applications. Still the efficiency of this kind of thermometry is rather low, since superfluid helium is an excellent coolant and lowers the efficiency of the thermo-devices. A complete thermal map of the cavity's surface, usually takes several cooling cycles of many hours. Multi cell structures, like the TESLA cavities, increase this effort even more, because more time or thermometers are needed compared to single cell cavities. Although in rf measurements one can determine quench locations, the quenching process usually starts at one single quench seed, down to one or two cells, by using different modes for the rf source, which depress the different cells with different loads.

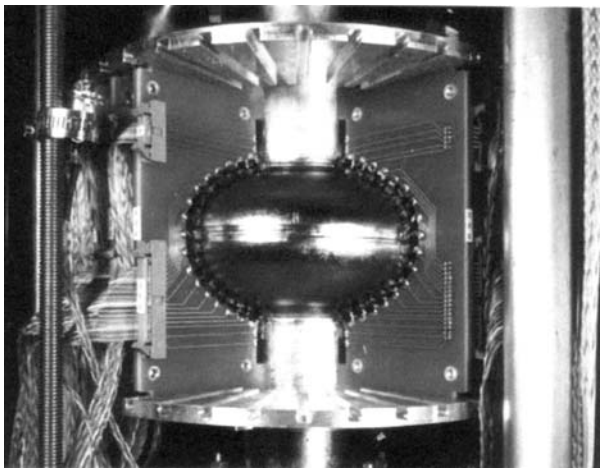

Figure 4.3.: Fixed thermometers at Cornell

Yet the advantages of such a mapping are clear: One would get information on the individual cells and their behavior under high loads and thus point out the weakest link responsible for the whole machines maximum gradient. Furthermore, in a next step, maybe after additional optical inspection, it is possible to fix problems with extra treatment and raise the gradient. But the disadvantages are obvious as well:

- several cooling cycles
  - lots of liquid helium needed
  - time-consuming
- practicability
  - setup of thermocouplers is rather complicated
  - for multi cell structures even more
- spatial resolution depends on resistor density

- effeciency is lowered by the coolant, ratio of detected temperature rise vs. actual temperature increase $20 - 30\,\%$ [8]

Thus one can summarize that the advantages gained by this analysis are excellent for cavity diagnosis and may even justify the detriments, but it would be desirable to reduce some of these obstacles. This may be possible in the future by using "Second Sound".

4.3. Second Sound

4.3.1. The Effect of Second Sound

Second Sound describes an alternative way of heat transfer somewhat similar to a wave propagation. The quantum mechanical effect is called second *sound* since it pictures a movement of density or entropy distributions in a wave like way much like the propagation of "normal" or first sound in air. Second Sound is quite well observed in a mixture of superfluid and normal fluid liquid helium, which is exactly the standard coolant for high frequency superconducting cavities. The phenomenon was predicted and theoretically described by L. Tisza in a phase model of liquid helium around 1940 and later by Landau. Experimentally it was proven in 1944 by V. Preshov. [3]

Table I. Second sound velocity *versus* temperature.

°K	meters/sec.
1.425	19.80
1.453	19.86
1.570	20.23
1.607	20.38
1.685	20.46
1.780	20.16
1.795	20.08
1.994	17.12
2.074	14.13
2.150	9.40

Figure 4.4.: Second Sound velocity

The most important results for the velocity of the heat propagation can be found in [3]. They are shown in figure 4.4. The authors come to the conclusion of a temperature dependency of the Second Sound given by:

$$v_{ss} = 2.6{\cdot}10 \sqrt{\frac{T}{2.19\,\mathrm{K}} \left(1 - \left(\frac{T}{2.19\,\mathrm{K}}\right)^{5.6}\right)} \left[\frac{\mathrm{m}}{\mathrm{s}}\right]$$

$2.19\,\mathrm{K}$ is the λ-point of helium. The function is derived from Tisza's theory and experimental results. A very good agreement is found with the data measured. In the actual thesis, the velocity taken into account for the cavity diagnosis is about $\approx 20\,\frac{\mathrm{m}}{\mathrm{s}}$ at $1.8\,\mathrm{K}$.

4.3.2. The Idea of Second Sound as a Cavity Diagnostic Tool

The basic idea of cavity diagnosis via Second Sound is rather simple or at least typical for modern physics, by using a quantum mechanical effect which fits perfectly into the experimental situation. The circumstances making the test situation suitable for the

effect of Second Sound are of course the presence of liquid helium at $\approx 2\,\mathrm{K}$ and the fact that a quench location or quench seed can be identified by its heat signature.

The setup is rather simple, a cavity is placed in a test stand, connected to an rf source and of course cooled down with liquid helium. While the field gradient is raised then, one is waiting for a quench at some level. The quenching spot heats up the liquid helium becomes the source of a Second Sound wave. This may sound simple, but is more complicated in practice. Test stands with liquid helium for the cavities are common yet, but to detect the Second Sound special detectors are required: Oscillating Superleak Transducers (OST). The experiments at Cornell University in 2008 are described in [7] and [22] and the results look quite promising. The project is very interesting, since it promises an easy way to detect quench locations. As seen in figure 4.5, a TESLA cavity has been successfully tested, which makes the project again very interesting for all people involved in the XFEL and ILC development.

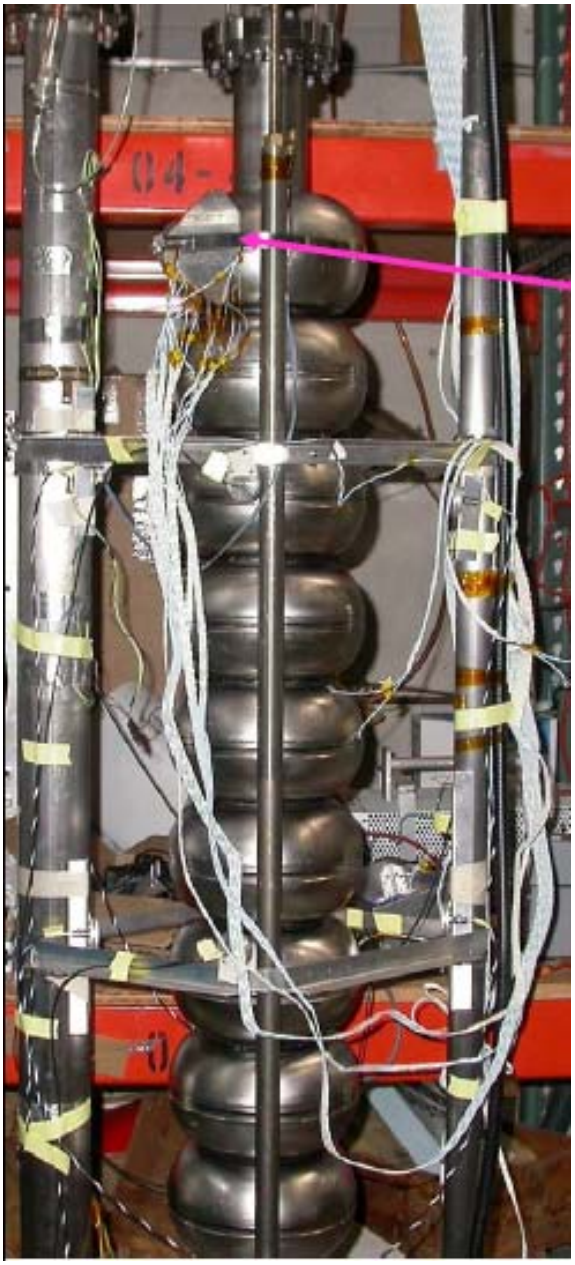

Figure 4.5.: TESLA cavity at Cornell, the arrow indicates the quench location. [7]

The setup of the experiment at Cornell involving the TESLA cavity used a kind of metal frame, shown in figure 4.5, with eight OSTs, one at each corner at the height of cell 3 and 8. The examined cavity quenched in cell one at $14.6\,\frac{\mathrm{MV}}{\mathrm{m}}$. It was tested three times, first without any detectors, a second time with the OSTs and in the third time with carbon thermometers. Although in the third run only a gradient of $8\,\frac{\mathrm{MV}}{\mathrm{m}}$ could be achieved, due to a problem with the input coupler, the thermometers delivered enough data to create a temperature map, which confirmed the quench location measured with the OSTs. Moreover an optical inspection of the critical area was performed and confirmed a defect within a circle with a radius of 3 mm around the point reconstructed via Second Sound.

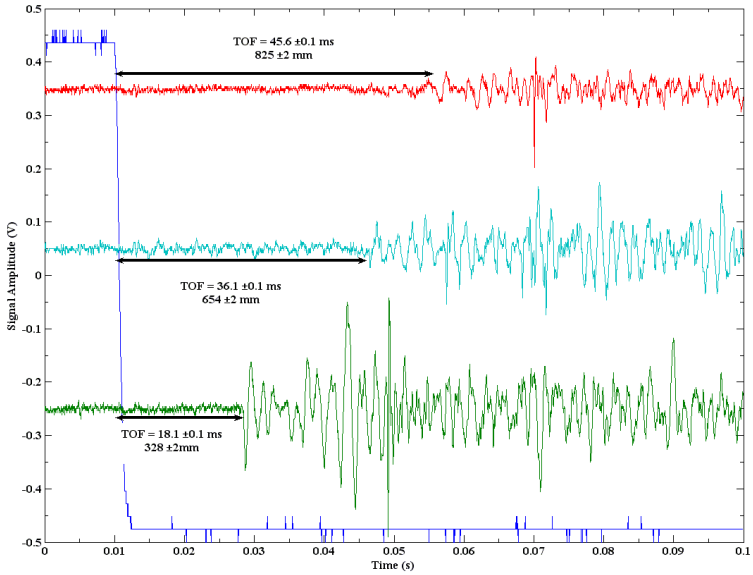

Figure 4.6.: Signals: Transmitted rf, OST 1, 2 and 3 [22]

The signals of the OSTs were triggered with the transmitted rf signal, as shown in figure 4.6. The combined information of the trigger, giving the point in time when the cavity quenches, and the "time of flight" of the Second Sound, made it possible to reconstruct the quench location using the Second Sound velocity at the current temperature. The response time of the OSTs is about 0.1 ms according to [7]. (The simulation of such events in a slightly different geometry and some possibilities of reconstructing the quench location will be discussed in part II of the thesis.)

4.4. Oscillating Superleak Transducers – OSTs

Oscillating superleak transducers can be used for excitation and detection of Second Sound in liquid helium. The concept is pretty similar to a speaker and a microphone (excitation ⇔ detection). The functional part is a nucleopore filter paper which contains small channels with a diameter of the order of $\approx 0.1\,\mu$m (see [6]). A very thin metal (gold in this case) layer is evaporated onto one side of the filter paper. This setup is able to detect the very little net mass flow induced by the Second Sound, by allowing the superfluid helium to pass through and by simultaneously stopping the normal fluid helium.

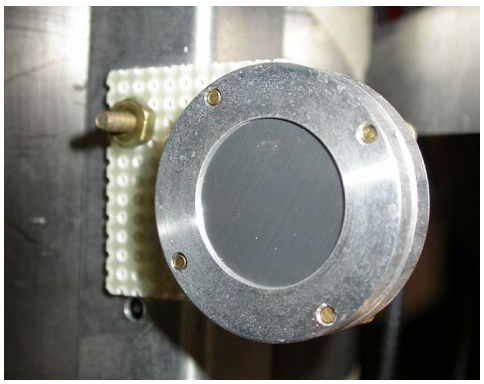

Figure 4.7.: An OST used for TESLA diagnosis at Cornell [7]

Part II.

Simulation

Chapter 5.

Simulation with MATLAB

5.1. Systematic Approach

The idea of the simulation part was to form a basic setup for a future test stand for TESLA cavities within a numerical routine. The TESLA cavities are chosen for this simulation as mentioned above on the one hand as a rather complicated example of a nine-cell structure and on the other hand to deal with an ongoing project of cavity quality diagnosis for the XFEL and ILC.

The purpose of the program is to examine the geometry of a possible diagnosis setup and to optimize it by simulating quenches, Second Sound signals and a reconstruction of quench spots. Therefore, the fundamental conditions and assumptions as well as the development of the algorithm have been developed after consulting of Prof. Dr. Eckhard Elsen, DESY, Hamburg.

The framework for the numerical routine has been MATLAB[1], a numerical computing environment by "The MATHWORKS", since it offers a large range of inbuilt functions and visualization tools. In principle, the very simulations could have been done with any other sophisticated programming environment or language, but the MATLAB language offered the quite comfortable advantage of vector based variables useful for this problem.

5.1.1. Creating a TESLA Cavity

The dimensions of the TESLA cavity were in agreement with [2] and are shown in figure 3.1, where the diameter of the iris diaphragms between the cells is 70 mm, the length of the structure is 1276 mm while the cells are 115.4 mm long and 206 mm wide each. The design of the cavity visualization should especially serve for a better understanding of probable reconstruction failures and the geometry of the problem. It needed to be adjusted to basic restrictions for the Second Sound measurements.

This is where the fundamental assumptions start to play a role. Firstly the stiffening rings and deep valleys in between the cells make it very complicated to get good Second

[1] Version 7.8.0.347 – R2009a, see [1, 16]

Sound signals from these regions. Secondly, one knows that the cell's equator welds are the most probable regions for material imperfections due to the fabrication process. Hence the possible quench regions can be limited to 84 mm wide regions surrounding the welds of each cell. This is not a random but pragmatic choice, since the cells outer regions have a bending radius of exactly 42 mm.[2] Taking all this into account, the cavity was approximately represented by a cylinder of height 1200 mm and nine half tori of torus radius 42 mm and central radius 61 mm (103 mm − 42 mm).

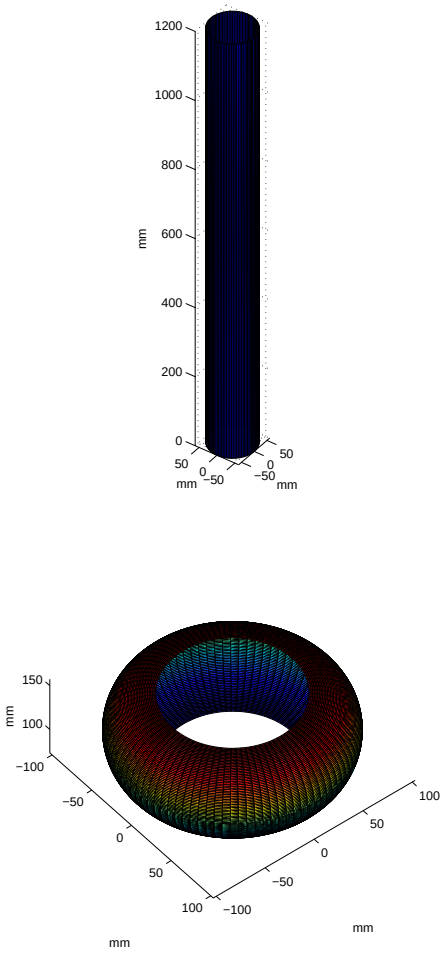

Figure 5.1.: The cylinder and the cell.

5.1.2. Concept of Simulating Second Sound

In the present case, the concept for the Second Sound simulation is based upon some kind of zeroth order approximation. Although the Second Sound has a strong wave character,

[2]The first and last half cell of a TESLA cavity have slightly different bending radii, but this is not expected to have any significant impact and is hence neglected in the simulation

we assume, that for a detection and reconstruction of quench spots, the direct lines of sight give the best signals and sufficient information. Additionally, the time of flight of the Second Sound – the time it takes to get from the quench spot to the OST– can be computed by threshold analysis as shown in figure 4.6.

The concept of the second part is basically to create random quenches on the cavity's surface, compute the direct lines of sight to any detector, include errors to the distance information given by these signals and finally to reconstruct the previously generated quench locations. So far, no experimental data was available for comparison.

5.1.3. Creating Quench Spots

When considering possible quench spots within the cavity structure there are two main factors characterizing the critical regions. The first is the accelerating field mode (TM_{010}) shown in figure 5.2 which has its field peak in the middle of each cell. The second factor has already been mentioned several times. The TESLA cells are produced as cups which are connected as dumb bells as shown in figure 5.3. These cups are welded to cells with an electron beam, but this welding process churns the niobium and may cause imperfections in the surface. Both factors make the cell's equator region the weakest link of the whole cavity. According to Prof. Elsen these regions always define the lower limits of the attainable field gradients.

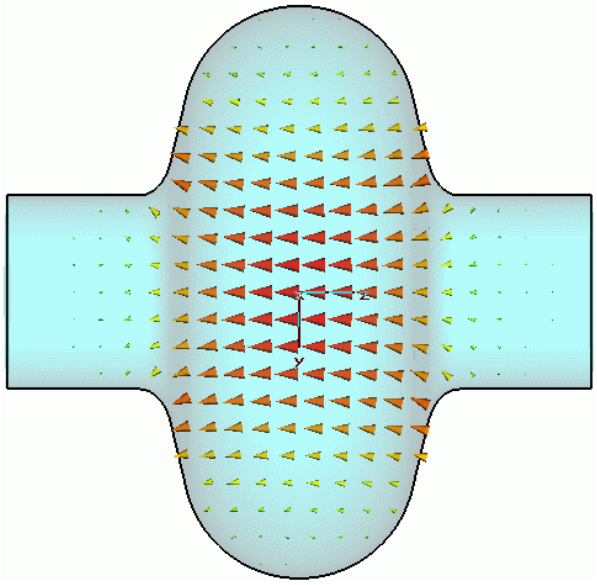

Figure 5.2.: $\vec{E}$-field in TM_{010}-mode [10].

Figure 5.3.: Dumb bell for TESLA cavity [4].

Due to these facts the generator creating arbitrary quench locations on the cavity's surface uses a normal distribution round the cell's equator and a uniform distribution around the whole cell's azimuth angle. In terms of cylinder coordinates this equals a normal distribution on the z-coordinate (with $3\sigma = 8\,\mathrm{mm}$ – width of the weld) and uniform distribution of the φ-angle. Both distributions used MAT-

LAB built-in random generators combined with a random integer generator choosing one out of the nine cells.

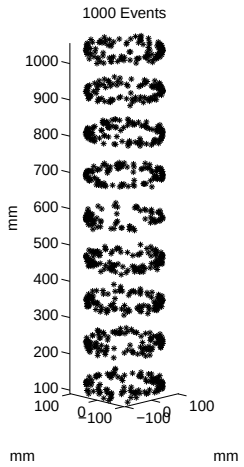

Figure 5.4.: 1000 generated quenches on the surface.

5.1.4. Detectors – OSTs

The placement of the OSTs or simply detectors for the Second Sound dictates principally nearly the entire following strategy. For a more realistic approach Prof. Elsen gave the advice to

- only install detectors on top and bottom of the cavity
- use a distance of the double cells radius (206 mm) from the cavity's center axis.

Both limitations are due to the geometry of the liquid helium tanks used for TESLA cavities. Furthermore, these limitations may change in different setups for simultaneous tests of more than one TESLA cavity, see outlook for more information. Especially the limitation to top and bottom positions differs from the Cornell setup (figure 4.5) and will complicate the data taking.

The number of detectors needed is the next figure of merit for the setup. In an earlier report, first considerations according to the number of detectors have been made in two dimensions, a typical concept with four detectors on top and four on the tank's floor. But it turned out that this setup in general gives too few signals for a working reconstruction process, compare figure 5.10. In theory, for such a process three or more signals together with the known cavity surface should return an unambiguous guess for the quench spot and two signals should return two candidates for a quench, while one signal alone would simply be impractical for any reconstruction. To solve the question, which minimum number of detectors could work under the given circumstances, an analytical, two dimensional reflection of the field of view of every detector is helpful:

It is easy to see that four detectors will not provide more than one signal for every position on the cavity, since at least for direct lines of sight every quench above a cell's equator should not be seen by a bottom detector and vice versa. One can show that six detectors would satisfy the requirement placed at the demanded distance of two cavity radii from the center axis. In a symmetric hexagon all angles are 120° and one obtains triangles upon connecting all the corners with each other, all with the same set of angles, 30°, 60° and 90°, as shown in figure 5.5. Using this, one can show that the connection of two opposing corners is cut into four parts of the same length by a circle around the hexagons center. Therefore, if this circle is identified with the cavity and the hexagons corners with the detectors, every point of the circle line is covered by an overlap of two detectors "visual field".

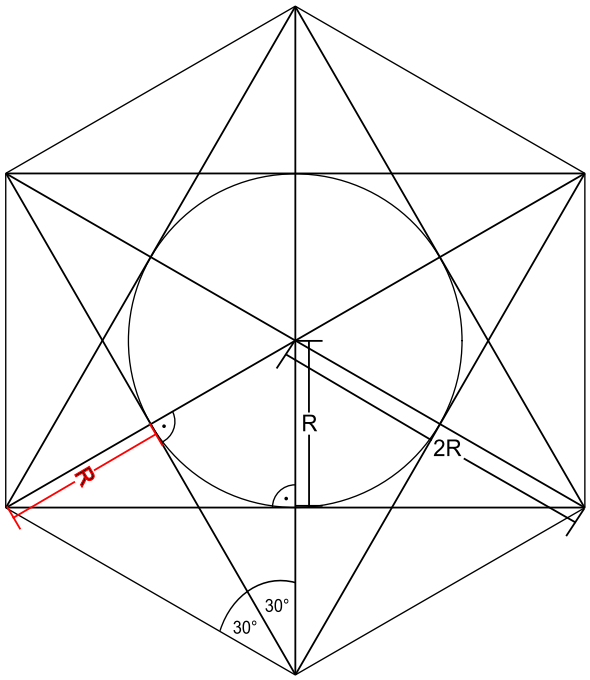

Figure 5.5.: Six detectors (corners) around the cavity (circle) in two dimensions.

These analytical considerations have led to the decision to mainly use a total of twelve detectors, six at the top and six at the bottom of the tank. For an even better spatial coverage, the two hexagons are in a twisted position against one other, so there is never a detector directly opposite to any other.

5.1.5. Computing the Traces

The next step in the simulation is trace elimination. Short loops have to be found in the routine which check if the possible connection of quench spot and detector is intersecting with the cavity's body. This is done by two major rules:

1. The "cylinder rule" and
2. the "next cell rule"

The Cylinder Rule

The basic concept of the "cylinder rule" is to create a cylinder around the cavity with the radius of the event, in other words to take the norm in the x-y-plane of the event (z-axis equals the axis of symmetry of the cavity) and to check if the connection to any of the detectors intersects with this cylinder.

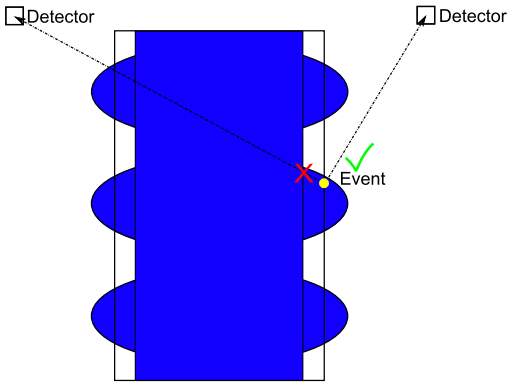

Figure 5.6.: Scheme of the "cylinder rule".

This verification is numerically done by connecting quench spot and detector and a comparison of the x-y-norm of the first entries. If the norm increases, the line is interfering with the cylinder; if not, it hits the detector directly. This is justified by the fact that all the detectors lie on a bigger radius than any of the events or quench spots. Figure 5.6 sketches two examples.

The Next Cell Rule

In combination with the "cylinder rule" the "next cell rule" examines intersections with neighboring cells as shown in figure 5.7 and the event cell itself. According to the problem's geometry, a direct connection between quench spot and detector cannot interfere with any other cell's surface if it does not with the direct neighbors of the quenching one. Computationally speaking, the "next cell rule" does a comparison of the x-y-norm of the connection line at the height of the next cell's equator (up and down) to the equator radius, therefore excluding any line of direct sight which intersects with other cells. For the self-intersection check the code does a check on the z-coordinate of the event and defines if it is below the equator of a cell and cannot be seen by top detectors and vice versa.

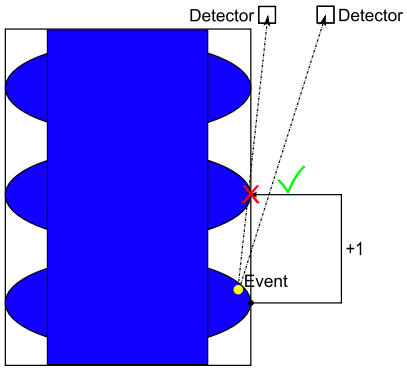

Figure 5.7.: Scheme of the "next cell rule".

In addition to these rules a kind of softening of especially the first one has been added, motivated by the wave character of the Second Sound and by some practical experience. This enhancement allows events within a distance of less than 20 mm to the cell's equator to "propagate" around it and still be seen by OSTs on the other side. Speaking in algorithmic terms this means that the self intersection test of the "next cell rule" is not performed for events within a distance of less than 20 mm to their cell's equator. This may be a first reason for possible errors in reconstructing the quench spots.

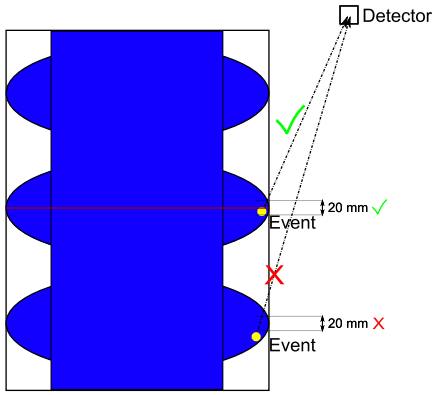

Figure 5.8.: Scheme of the free propagation area around the equator.

5.1.6. Contribution of Errors

While producing all data of the connection lines, the systematical inclusion of a distance or "time of flight" dependent error is a link between simulation and experiment. Since no comparison with any investigations of Second Sound damping and typical errors within the possible test setups was possible yet, an error of approximately $4 - 6$ mm over the distance of half a meter was assumed and included in an exponential growth formula:

$$\text{error} = 4\,\text{mm} \cdot \exp\left(\frac{\text{distance [in mm]}}{1000\,\text{mm}}\right) \tag{5.1}$$

The actual error in the information gained by the signals is then simulated in such a way, that a random number of a normal distribution around zero with the error equaling the standard deviation is added to the real distance to imitate an experimental "measurement". The result for one event with a real distance of ≈ 536 mm is depicted in figure 5.9.

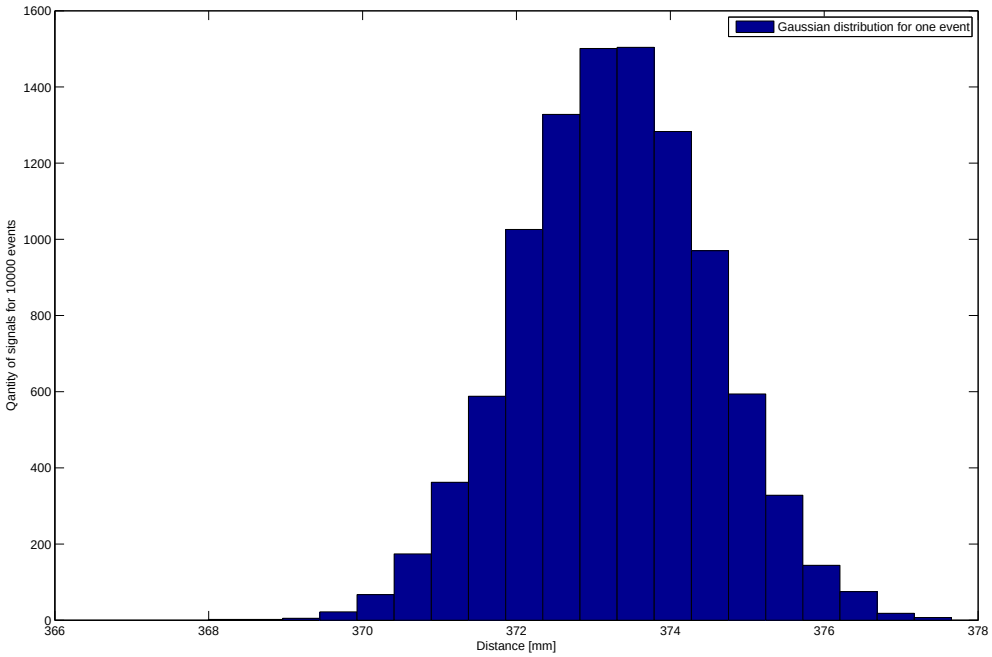

Figure 5.9.: Error distribution for one event with a distance value of $\approx 372.5\,\text{mm}$. The error for the *same* event has been generated 1000 times. This shows the GAUSSIAN distribution of the error.

5.2. Analysis

5.2.1. Signals per Event

As a first analysis, the trace elimination rules, computing the straight connections, were used to verify the conclusion that six detectors at each of the two levels, top and bottom of the tank, would return the postulated two signals per event at least. Figure 5.10 shows the results of this analysis and justifies the conclusion of 5.1.4, for twelve detectors a ratio of approximately 2.4 signals per event can be achieved. Therefore in the following analysis and calculations, twelve detectors have been chosen for any evaluation of the generated data. This seems to be the reasonable minimum number of detectors useful under the chosen conditions for a Second Sound analysis.

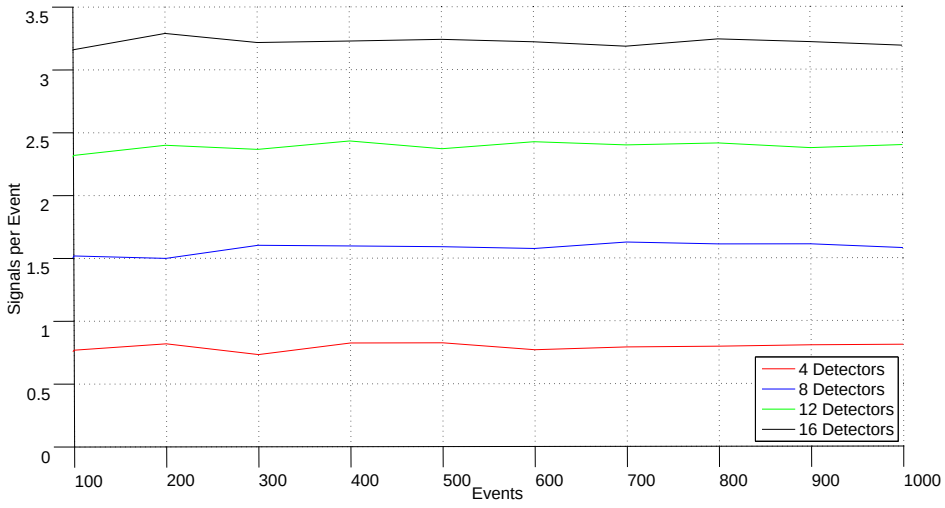

Figure 5.10.: Comparison of the signal per event rate from 4 to 16 detectors, tested with 100 to 1000 events (in steps of 100 events).

5.2.2. Events with two Signals

Quenches which produce only a single signal are possible due to the cavity's geometry, but nevertheless unusable for reconstructing the quench spots. Such a case may occur if a spot lies directly in front of a detector, above or below the weld. Therefore a reasonable reconstruction process requires two signals per event. While for a quantity of three signals or more a NEWTON-RAPHSON-method was used to reconstruct the event. This numerical approach turned out to be slightly divergent in a lot of the "two-signal" cases, since too little information is contained in just two distances.[3] But still one has to distinguish, especially in the case of two signals, the position of the detectors which have direct sight onto the event, as shown in figures 5.11 and 5.12. From the point of view of the OSTs, only two pieces of information are known, the distances to the event and which detectors have registered the event in direct lines of sight. For two direct hits, one can create two spheres around the detectors, whose radii are equal to the measured distance. The spheres overlap, giving an intersection circle, which can be calculated algebraically. In combination with the constraint that the quench source is placed on the cavities surface, this circle submits up to four possible quench spots with the cavity. In the case of four intersection points, two of these can always be excluded, since they lie on the opposite side of the cavity and therefore cannot be observed by the detectors. Thus, in the majority of the cases two intersection points are left.[4]

[3] This method could be improved by *direct* inclusion of constraints, such as the event being on the cavities surface.

[4] In the case of just one intersection the reconstruction is of course complete.

These events can be divided into two cases:

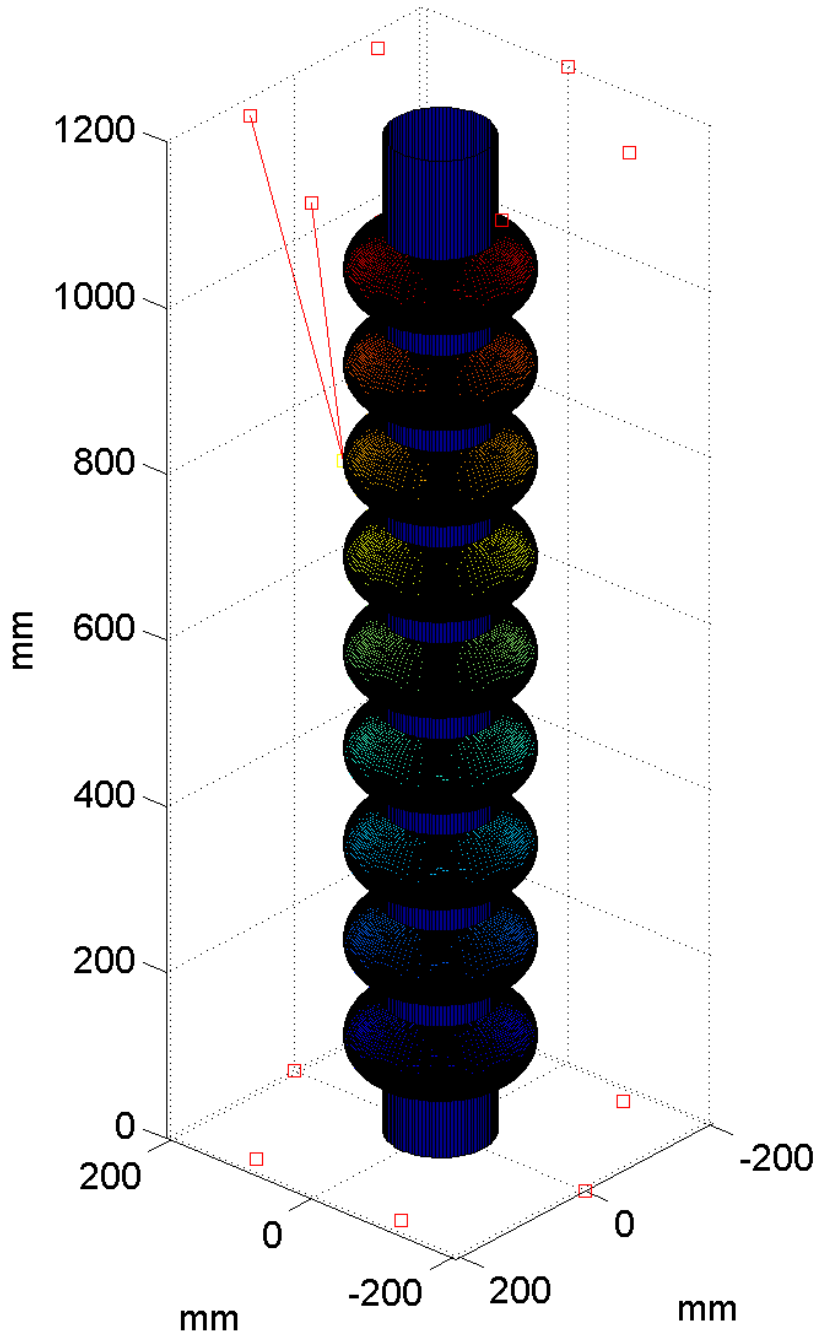

Figure 5.11.: An example of a "two-signal" event, reported by detectors in the same plane.

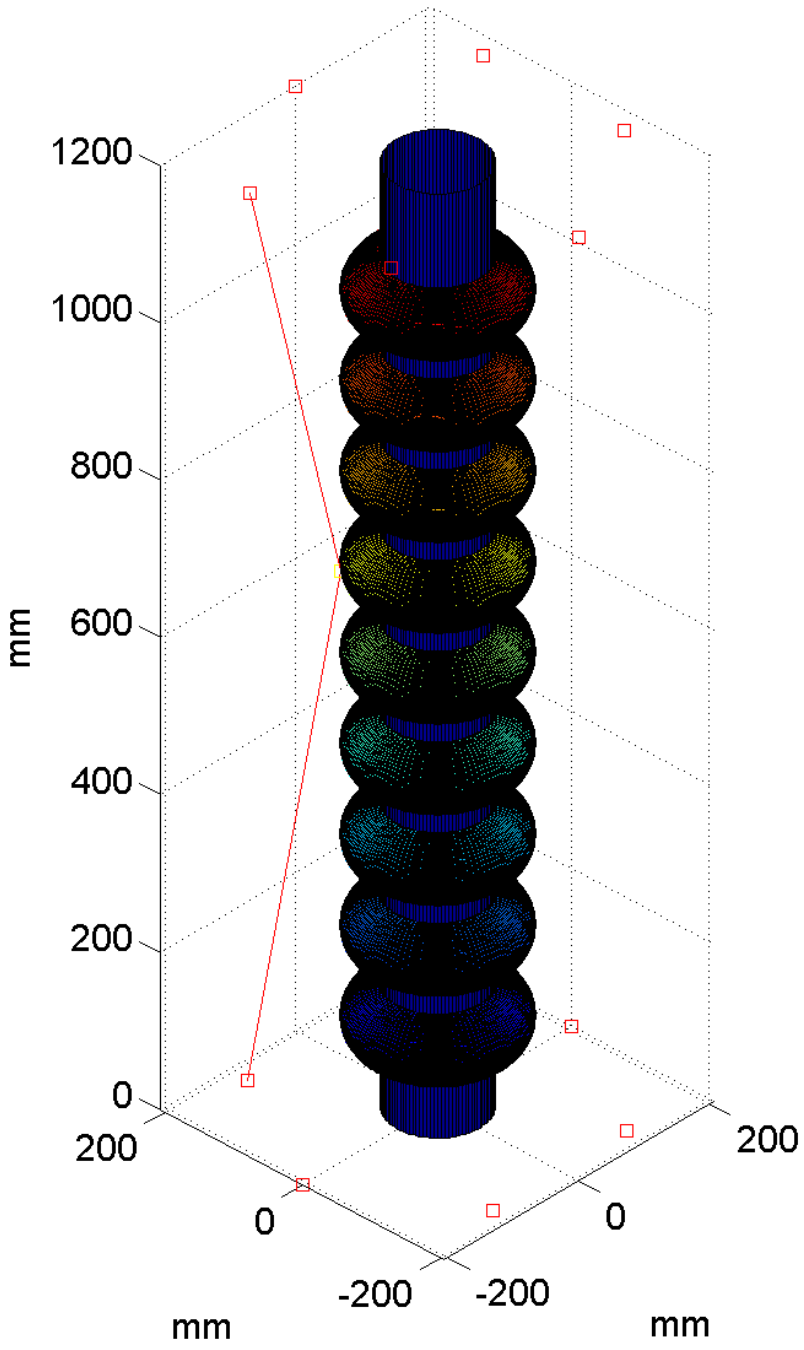

Figure 5.12.: An example of the critical case, in which two detectors of different planes detect the event.

In the case that the two responding detectors are in the same plane, top or bottom of the tank, the circle is parallel to the cavity's axis. So any point of intersection of the cavity and the circle is on the opposite side of the cavity, which is the blind side for the detectors, or is actually the quench spot. The circle cannot have two intersection points with the cavity on the detector facing side of the surface, because the center of the circle lies in the same plane as the top or bottom of the entire cavity.[5]

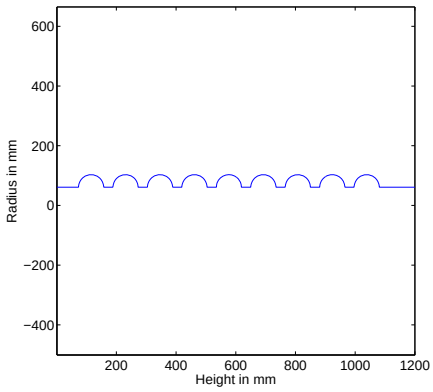

Figure 5.13.: The function "teslaradius" in dependence of height z

These events can be handled by an iterative algorithm, which again consists of a comparison of the x-y-norm of the points on the circle of intersection and the associated value of the function "teslaradius" illustrated in figure 5.13. "teslaradius" takes the z-value of any point and returns the radius of the cavity at that height.

The second case of two detectors, one at the top, one at the bottom, returning a signal, is unfortunately slightly more complicated. The reconstruction process of the previous problem can be used for this case as well *but* it will return up to two equal points of reconstruction with, depending on the individual errors, different deviations from the original quench spot. Without any further information, the algorithm cannot discriminate between these two points. A very good example is shown in figure 5.14. Both points are equal within the error of the "measured" distances. As a short preview of the final conclusion, one can summarize for this case of event, that the result is not optimal but still satisfying. Two possible locations are returned, narrowing down the candidates for a quench. These two positions can be further examined, for example by an optical inspection, to verify the real quench position and to find the reason for the superconductivity's breakdown.

[5] One might say that the circle would intersect with the cavity's surface in a second point mirrored on the detector's plane.

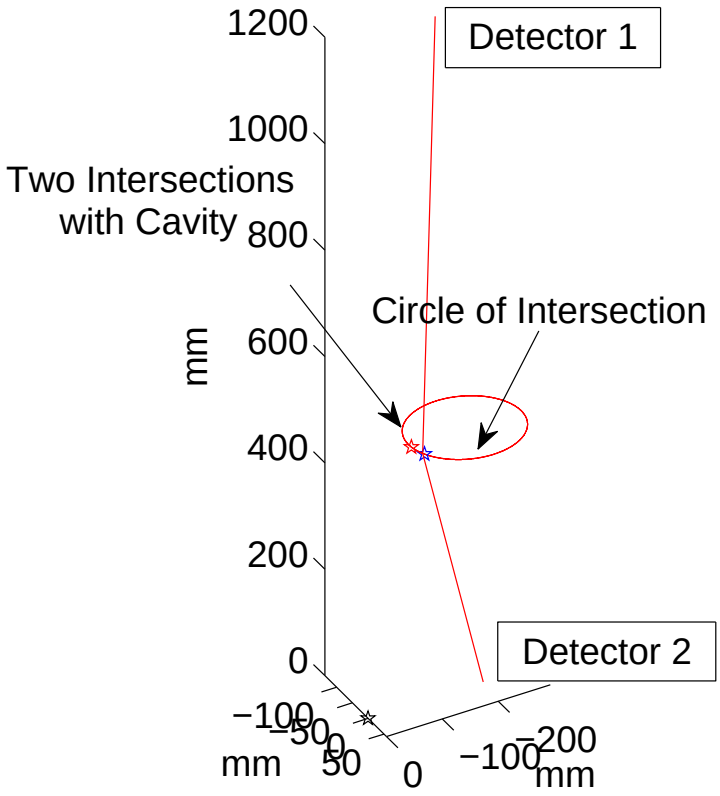

Figure 5.14.: A "two-signal" event returning two possible locations.

5.2.3. Events with three or more Signals

Due to the wave propagation rule and the concentration of the generated events on the cell's equator welds, a lot of the quench spots have connections of direct sight to three detectors, some of them even to four. In these cases a variation of a NEWTON-RAPHSON iteration was used. It is also known as the method of the "least squares". The concept is to save the position of the responding detectors, $\vec{x}_i$, and the related distance information, d_i. Then the χ^2 distribution is given by:

$$\chi^2 = \sum_i \left(\frac{|\vec{q} - \vec{x}_i| - d_i}{\sigma_i} \right)^2$$

Where σ_i are the errors of every distance information, computed with equation 5.1 and the index i goes from one to the number of signals. In a numerical realization, the algorithm starts with a guess for $\vec{q}$, the quench location, and tries to find a minimum for χ^2 by applying little changes on $\vec{q}$. Therefore the mentioned NEWTON-RAPHSON method was used, as it approximates the roots of a real-valued function and in this case

the roots of the derivative of the χ^2 expression giving the minimum of the function. The iterated final outcome lies, due to the included errors, somewhere close to a cell's surface. With the distance to the next point of the cell's surface at the same height, one can find the closest point on the cavity's surface, by going up and down this surface, cheking if the distance in- or decreases. This is done again with the "teslaradius"-function, see figure 5.13. The closest found point on the cavity's surface gives the finally reconstructed quench spot.

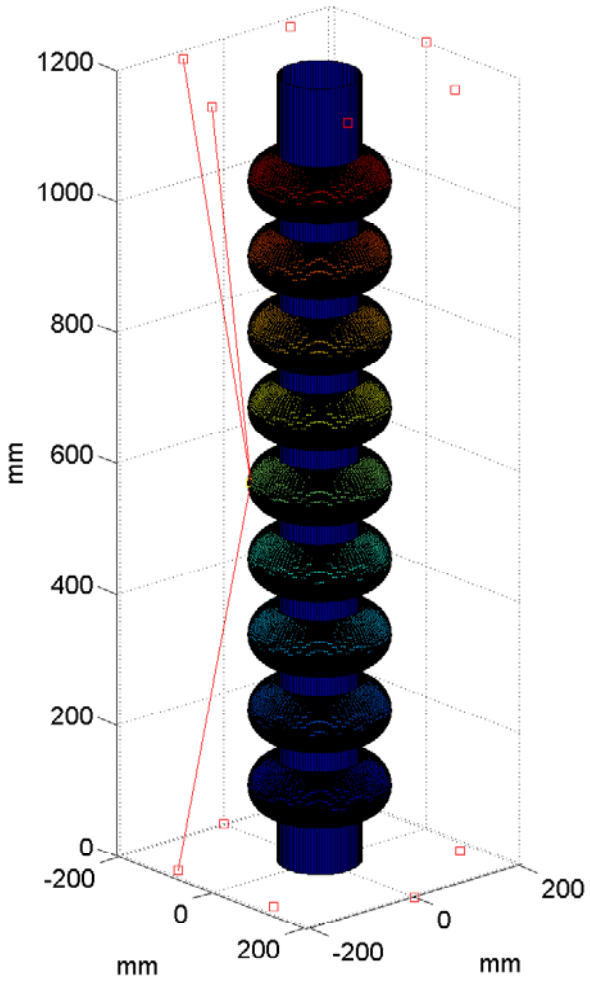

Figure 5.15.: A typical "three-signal" event.

5.2.4. Statistical Analysis

For the further analysis a bigger set of data was produced by the "quench generator". The set contained 2000 events. The first step was to analyze the capability of the

detector setup to establish lines of direct sight on these events according to the above explained rules of trace elimination. Despite the fact that the limitations in placement[6] due to the tank's structure may have reduced the detector's view, still only 23 events were seen by one OST only. In other words, 98.85 % of the events returned sufficient information to be reconstructed to at least two quench spot candidates:

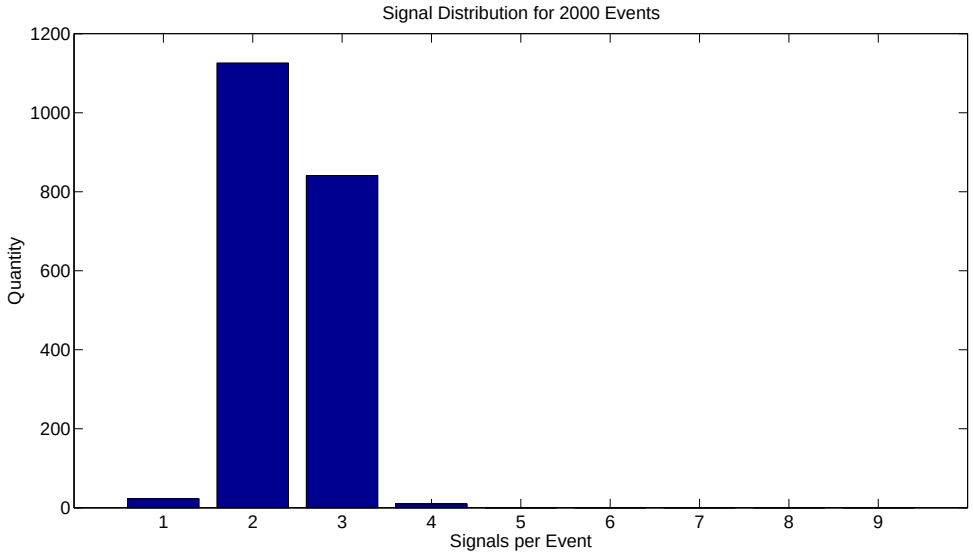

Figure 5.16.: Histogram of the signals-to-event ratio for the 2000 generated quench spots.

The majority of the events was reported, as expected, by two detectors, but still a huge number by three. The precise result was:

Number of Signals	Quantity in 2000 events	Percentage
1	23	1.15 %
2	1127	56.35 %
3	840	42 %
4	10	0.5 %

With this wealth of data, the signals were used to reconstruct the quench spots with the methods explained earlier. The aim was to find out what the actual spatial resolution of the measurement was. Since an arbitrary amount of error had been added to every signal, one could predict a statistical error but nevertheless the experimental results may differ, depending on the true limitations imposed by electronics and the cavity test stand's dimensions. The deviation Δ of the reconstructed quench spots was computed

[6]Detectors are only placed at height 0 and 1200 and at a distance of only $R = 103\,\text{mm}$ to the cell's equators.

with the original data of the quench spots which was saved within the generating process:

$$\Delta = |\vec{q}_{\text{real}} - \vec{q}_{\text{recon}}|$$

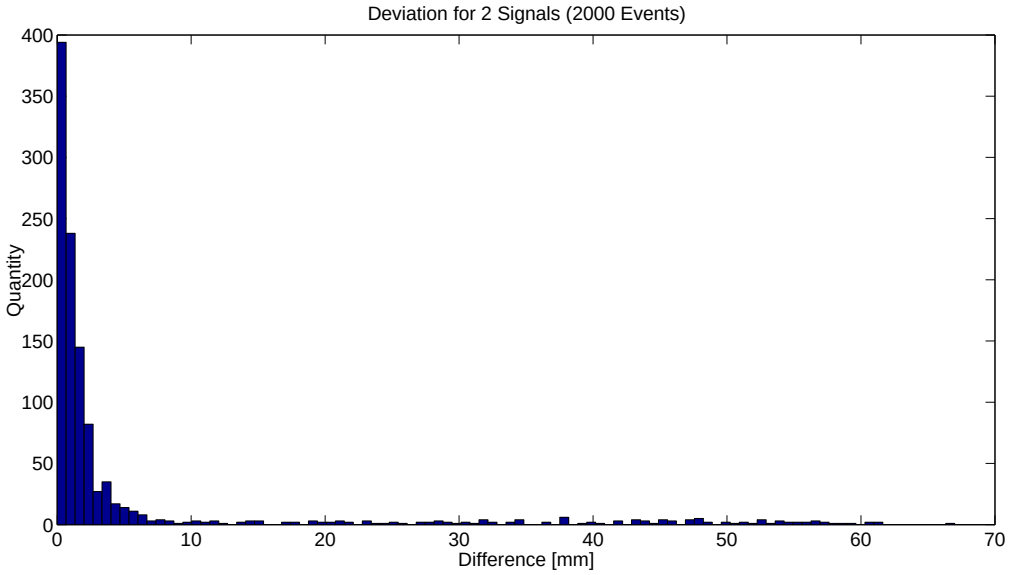

Figure 5.17.: The histogram of the deviation Δ of reconstructed quench spots returning **two** signals according to the setup.

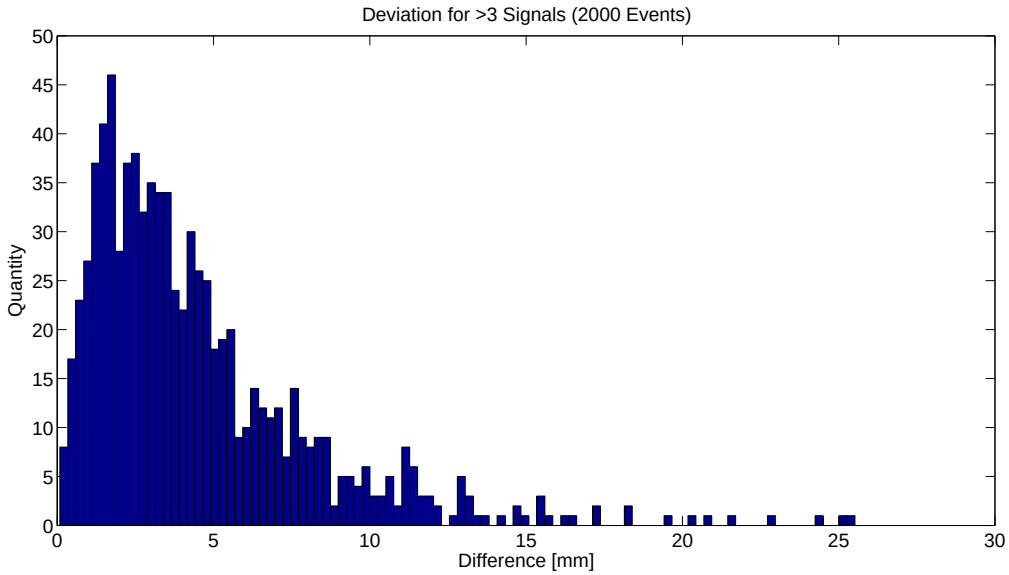

Figure 5.18.: The histogram of the deviation Δ of reconstructed quench spots returning **three** or more signals according to the setup.

From the histograms 5.17 and 5.18 one can see, that the distribution of the "two-signal" events has a very long tail of reconstructed events with quite a large deviation from the real event. This is of course explained by the reconstructions where two possible quench locations are returned. These cause the big standard deviation and variance for the "two-signal" case. The distribution for the "three-signal" events shows far fewer variations. The maximum here is around a value of $\approx 1.9 - 2\,\text{mm}$, this is probably due to the fact that the variations in the iteration of the NEWTON-RAPHSON are linked to the errors of the distance information. But still the values are quite good and remain within an acceptable range, especially for the events with three signals. The numbers of the distributions confirm the first impression:

All values in mm	**Two** Signals	**Three** Signals
Mean Value	5.6822	4.5217
Standard Deviation	12.8498	3.6990
Variance	165.1168	13.6822

The fluctuations are not very low, probably due to the generously estimated errors, but as the mean values are of the order of only a few millimeters they are promising towards the advantages of the shown technology. Further optimization of the reconstruction method and the technical setup may reduce these values even more.

Chapter 6.

Conclusion and Outlook

6.1. Conclusions

The first analysis of simulated events is primarily an examination of characteristics of the number of signals achieved by the number of installed detectors. The result was that, in the chosen case of six detectors at two levels, events are in general detected by two or by three OSTs with straight lines of sight. One may perform further investigations on the dependence of the number of signals on the quench spot's location. For example in the case of only one signal, the quench is probably directly facing the only responding detector and could therefore also be reconstructed with its distance information. Such additional examinations should also be done in advance to any quality checking in agreement with the existing geometry of the test stand. Yet any solution has to be rather universal since the chance to have a quench being in any of the cells remains the same for the entire cavity.

The crucial two-signal case, which is predominantly observed for events on the middle cells, will return two results without an easy possibility to discriminate between them and find the actual failure. This demonstrates a need for further diagnostic methods, which will of course always be part of any future quality analysis for cavities. The errors of the reconstruction mode are in general surprisingly low ($\approx 5.7\,\mathrm{mm}$). In a lot of the cases, one of the guesses is within a few millimeters from the original quench spot (compare figure 5.17), so the reasons for the specific quench can be located quite precisely.

It comes as no surprise that in the case of three or more signals, the statistical analysis shows less fluctuation around a value of 4.5 mm than with only two signals. This indicates that more detectors returning more signals will result in even more precise reconstructions. This is of course limited by the cavity's and the liquid helium tank's geometry and the placement of the detectors. For example the error of the distance information by threshold analysis on the cells $4-6$ could be tremendously decreased with detectors at the middle of the cavity, compare the setup at Cornell figure 4.5.

Finally, the simulation shows that it is possible to cover nearly 99 % of the critical regions of a TESLA cavity with a *small* number of detectors. And it promotes the idea of

Second Sound diagnosis. Since the aim of this thesis was to present the method "Second Sound as Cavity Diagnostic Tool" and to examine the possibilities of this procedure with an example project – the TESLA cavities – the results show, that the advantages gained by this method are confirmed. In comparison to current methods, where random samples of cavities are tested because the diagnosis procedure takes to much time, Second Sound marks a huge progress and will probably play an important role in superconducting cavity diagnosis.

6.2. Outlook

Fixed Conditions of the Model

Before the simulation was set up several assumptions had been made and additionally certain terms of the geometry had been defined. For a future application of this diagnostic tool some of these restrictions will probably have to be abandoned.

Zeroth order Approximation For the reconstruction of quench spots only lines of direct sight were used. Other signals are very likely and may improve the information obtained by the detectors.

Critical Region The equator area of every cell is regarded to be the main source of quenches, since its weld is the main reason for material disorders.

Form of the Cavity The cavity has been approximated by a cylinder and nine half-tori, which still covers at least the critical regions quite well. All additional parts like HOM couplers were neglected.

Position of the Detectors The OST placement was limited to just the top and bottom level of the cavity's tank and furthermore to a distance of 103 mm from the cell's equator, which is twice the maximum radius of the cavity.

Velocity of Second Sound The velocity of the Second Sound has been assumed to be constant at least. According to Zachary Conway at the Cornell experiment, special attention has been paid to perform the measurements at constant temperatures. This seems to be quite reasonable and important for the sensible measurements.

Error The time resolution at Cornell has been about ≈ 0.1 ms, which correlates to a spatial resolution of about 2 mm for a Second Sound velocity of $20\,\frac{\mathrm{m}}{\mathrm{s}}$. In the simulation a distance dependent error was assumed, which is about ≈ 5 mm for a distance of half a meter. Still more precise measurements on the error have to be made.

Further Diagnosis Methods

In addition to the method described of using Second Sound for a quench spot determination further diagnosis methods can be applied. For example an optical inspection of the Cavities is a promising way to determine the actual imperfections on the cavity's surface and was used in the Cornell experiment. Besides a plain operation of the cavity in the π-mode just delivers the very first failure for a quench, so the weakest link in the chain, since the peak field in every cell is the same in this mode. By using different modes, different loads could be tested in the individual cells. This may enable the capability to find several impediments for a high field gradient in one cooling cycle via Second Sound.

Future Test Stand at DESY

DESY is currently building the XFEL, the TESLA cavities for the main linac should arrive in late 2010. Although the intended gradient is "only" 23.6 $\frac{\mathrm{MV}}{\mathrm{m}}$ the cavities need to be tested soon. The intention is to use Second Sound at this project to improve the data acquisition. The existing test stands and applications will lead to further restrictions for the set up. For example, a test stand with four cavities is planned to accelerate the diagnostic process. This geometry sets a lot of new conditions and possibilities for the placement of the detectors.

Bibliography

[1] O. Beucher. *MATLAB und Simulink*. Pearson Studium, 3^{rd} edition, 2006.

[2] TTF Collaboration. Superconducting tesla cavities. *Physical Review special Topics - Accelerators and Beams*, 3, 2000.

[3] W. M. Fairbank C.T. Lane, H. A. Fairbank. Second sound in liquid helium ii. *Physical Review*, 05, 1947.

[4] J. Delayen. Cavity fabrication. Technical report, Thomas Jefferson National Accelerator Facility Old Dominion University, June 2008.

[5] M. Altarelli et al, editor. *European XFEL - Technical Design Report*. DESY XFEL Project Group European XFEL Project Team Deutsches Elektronen-Synchrotron Member of the Helmholtz Association, 2007.

[6] F. Pobell G. Zimmermann. Investigations of oscillating superleak second-sound transducers. *Journal of Low Temperature Physics*, 61, 1985.

[7] D. Hartill. Second sound as a cavity diagnostic tool. Jefferson lab seminar, Cornell Laboratory for Accelerator-Based Sciences and Education, 2008.

[8] H. Padamsee J. Knobloch, T. Hays. *RF Superconductivity for Accelerators*. Wiley-VCH, 2^{nd} edition, 2008.

[9] ANL J. Norem, M. Pellin. Gradient limits and scrf performance.

[10] A. Labanc. Electrical axes of tesla-type cavities. *TESLA Report*, 1, 2008.

[11] L. Lilje. Superconducting radiofrequency accelerating structures. 2008.

[12] N. Walker N. Phinney, N. Toge, editor. *International Linear Collider Reference Design Report*, volume Volume 3: ACCELERATOR. International Linear Collider Collaboration, 2007.

[13] H. Padamsee. *RF Superconductivitiy*. Wiley-VCH, 1^{st} edition, 2009.

[14] H. Podlech. Hochfrequenzparameter. 2007.

[15] P. Schmüser. Superconductivity in high-energy particle accelerators. 2009.

[16] W. Schweizer. *MATLAB kompakt*. Oldenbourg Verlag, 3^{rd} edition, 2008.

[17] J. Sekutowicz. Superstructures. November 2002.

[18] R.L. Geng V. Shemelin, H. Padamsee. Optimal cells for tesla accelerating structure. *Nuclear Instruments and Methods in Physics Research*, 2003.

[19] R. Kleiner W. Buckel. *Superconductivity: Fundamentals and Applications*. WILEY-VCH, 2^{nd} edition, 2004.

[20] W. Weingarten. Rf superconductivity for accelerator application. Seminar at GöttingenUniversity.

[21] K. Wille. *Physik der Teilchenbeschleuniger und Synchrotronstrahlungsquellen*. Teubner B.G. GmbH, 2^{nd} edition, 1992.

[22] H. S. Padamsee Z. A. Conway D. L. Hartill. Oscillating superleak transducers for quench detection in superconducting ilc cavities cooled with he-iis. *TTC-Report*, 06, 2008.